ELECTRODEPOSITED CdTe AND HgCdTe SOLAR CELLS

BULENT M BASOL

International Solar Electric Technology (ISET), 8635 Aviation Blvd , Inglewood, CA 90301 (U S A.)

(Accepted September 17, 1987)

Summary

The processing steps necessary for producing high efficiency electrodeposited CdTe and HgCdTe solar cells are described. The key step in obtaining solar cell grade p-type CdTe and HgCdTe is the "type conversion–junction formation" (TCJF) process. The TCJF process involves the heat treatment of the as-deposited n-type CdTe and HgCdTe layers at around 400 °C. This procedure converts these n-type films into high resistivity p type and forms a rectifying junction between them and the underlying n-type window layers. Possible effects of oxygen on the TCJF process are discussed. The results of studies made on the structural, electrical and optical properties of the electrodeposited CdS, CdTe and HgCdTe films are presented. The resistivity of the electrodeposited HgCdTe can be made lower than that of CdTe. Consequently, solar cells made using the HgCdTe films have, on the average, better fill factors than those made using the CdTe layers. HgCdTe is also attractive for tandem-cell applications because of its variable band gap which can be easily tuned to the desired value. CdS/CdTe and CdS/HgCdTe heterojunction solar cells with 10.3% and 10.6% efficiency have been demonstrated using electrodeposition techniques and the TCJF process.

1. Introduction

CdTe, with its near-ideal band gap and high optical absorption coefficients, is a promising compound semiconductor for low-cost thin film solar cell applications [1]. Polycrystalline thin films of CdTe have been successfully prepared by a variety of techniques such as vacuum evaporation [2, 3], sputtering [4], close-spaced vapor transport (or sublimation) [5, 6], screen printing [7], spraying [8], chemical vapor deposition [9] and electrodeposition [10, 11]. Although all the methods listed above can, under properly monitored growth conditions, produce single-phase CdTe films, so far the best solar cells have been obtained using films prepared by close-spaced vapor transport (or sublimation), screen printing, chemical vapor deposition and electrodeposition techniques. These devices were all

0379-6787/88/$3.50

Cd(Zn)S/p-CdTe-type heterojunctions and they have demonstrated over 9% conversion efficiency. Recent reviews of thin film CdTe solar cells can be found in refs. 12 - 14.

$Hg_{(1-x)}Cd_xTe$ (or HgCdTe) is a very important material for IR detector technology and a considerable amount of research has been done on the mercury-rich compositions of this compound [15]. It was only recently, however, that the cadmium-rich compositions of HgCdTe were successfully utilized in making high efficiency thin film solar cells [16 - 20]. A demonstration of 10.6% efficiency in the electrodeposited CdS/HgCdTe heterojunction structure [20] established HgCdTe as a viable polycrystalline thin film solar cell material. HgCdTe has a number of attractive features. Firstly, the optical band gap of this material can be tailored by adjusting its stoichiometry. This property is important for the design and fabrication of high efficiency tandem structures where the bottom cell is made of HgCdTe. Furthermore, the resistivity of p-HgCdTe can be lower than that of p-CdTe Therefore contacting this material is easier than contacting p-CdTe

Electrodeposition is a very attractive method for thin film solar cell processing. It is a simple technique which lends itself to large-scale production. It does not require specialized expensive equipment. Material utilization in the electrodeposition technique is extremely good since plating takes place only on the substrate. Electrodeposition can produce high purity materials if special attention is paid to the purification of the plating solutions which can be achieved by pre-electrolysis.

In this paper, we review the pioneering work undertaken during the last decade by Monosolar Inc. in developing the electroplated CdTe and HgCdTe thin film solar cells, especially the very promising CdS/CdTe and CdS/HgCdTe heterojunction structures. Section 2 is a brief overview of the initial research which resulted in the development of the cathodic electrodeposition technique for CdTe and the demonstration of the first Schottky barrier solar cells made on this material. In Section 3, the electrodeposition technique for CdS, CdTe and HgCdTe thin films and Monosolar's "type conversion–junction formation" (TCJF) process are described and the contacting procedures for the devices are discussed. Results of the film characterization studies are presented in Section 4. Finally, the performance of the electroplated CdS/CdTe and CdS/HgCdTe devices are reviewed in Section 5.

2. Background

Research on the cathodic electrodeposition of CdTe for solar cell applications was initiated by Monosolar Inc. in 1976, under a contract from the Energy Research and Development Administration (ERDA) [21]. The initial work at Monosolar and its subcontractor, the University of Southern California (USC), concentrated on the development and the understanding of the cathodic electrodeposition technique for CdTe [10, 11]. This was followed by the demonstration of a limited photovoltaic activity in glass/

indium tin oxide (ITO)/CdTe/Te-type structures where both CdTe and tellurium were electrodeposited (see for example ref 21). Although films 1 - 2 μm thick were relatively easy to plate on metallized substrates at that time, uniform and pinhole-free CdTe layers could be deposited on ITO-coated substrates to a thickness of only 0.1 - 0.2 μm. The resulting devices were Mott barriers and their demonstrated efficiency by mid-1978 was about 1.25% [22]. The Monosolar and University of California, Los Angeles, (UCLA) team started to work on a joint program supported by the Solar Energy Research Institute (SERI) in 1979. This project was aimed at the identification and evaluation of the mechanisms limiting the efficiency of electroplated CdTe cells, the reduction in the pinhole density in CdTe films and the development of Schottky barrier and heterojunction devices on these films [23]. During the course of this research effort, important electrical and optical properties of electrodeposited CdTe thin films were determined [24 - 27] and the first Schottky barrier solar cell on this material was demonstrated and reported [24, 28]. This device was a Au/n-CdTe/ITO/glass Schottky barrier and its conversion efficiency was improved to around 6% by mid-1980 [29] by interjecting a thin (about 500 Å) CdS film between the ITO (0.4 μm) contact and the CdTe layer (0.8 μm) and by annealing the device at around 250 - 300 °C before the evaporation of a gold barrier layer 50 - 100 Å thick. The thin CdS buffer layer in this cell served as the ohmic contact to the n-CdTe film and it allowed the structure to be annealed without producing pinholes in the CdTe film and without giving rise to the resistive oxide layer which would otherwise form at the CdTe/ITO interface [29]. The observed improvement in the Au/n-CdTe/CdS/ITO/glass back-wall Schottky device was due to the better collection efficiency observed in this annealed structure. The electrodeposited CdTe Schottky barriers were further improved by the Ametek group utilizing similar heat treatment steps and a cadmium contact [30].

The limitations on the efficiency and the stability of Schottky barrier solar cells are widely known. It was for this reason that research at Mono-

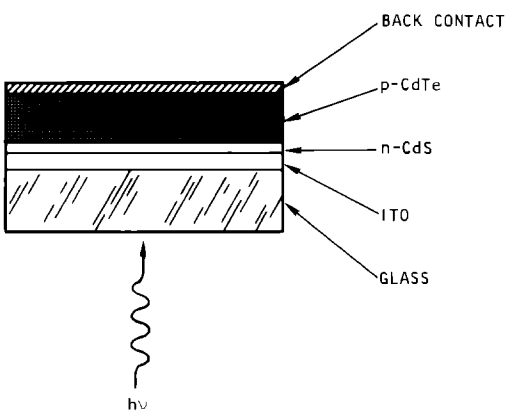

Fig. 1. The electrodeposited (Hg)CdTe/CdS solar cell structure

solar concentrated on the more promising heterojunction structure shown in Fig. 1. The TCJF process was developed and patented [31] making it possible for the first time to produce efficient CdS/p-CdTe solar cells using electroplated films [31 - 35]. Electrodeposited HgCdTe was also developed and demonstrated to be a viable solar cell material [16 - 20].

3. Film preparation

3.1. CdS deposition

The CdS electrodeposition bath consists of a $CdCl_2$ solution (0.1 - 0.5 M) containing sodium thiosulfate (0.01 M). The deposition potential is kept at about −0.65 V with respect to a standard saturated calomel electrode. The electrolyte is stirred and heated to 85 - 90 °C. The typical plating current density is about 0.03 mA cm^{-2}. The deposition rate is around 15 Å min^{-1}. Well-adhering CdS films 500 - 1000 Å thick can be plated on metallic surfaces or surfaces coated with a transparent conductive oxide (TCO).

3.2. CdTe deposition

The cathodic electrodeposition of CdTe from acidic solutions containing Cd^{2+} and $HTeO_2^+$ was first achieved by the Monosolar–USC team [10, 11]. Since then, only minor adjustments have been made to the composition and the pH of the plating electrolyte.

The electrolyte typically contains 0.5 M $CdSO_4$ and about 30 - 40 ppm of $HTeO_2^+$. The pH of the solution is adjusted to 1.6 using H_2SO_4. Two anodes, one of tellurium and the other of carbon, are used. Either one of these anodes is switched into the circuit during plating using a timer switch. When the current is passing through the tellurium anode, $HTeO_2^+$ is injected into the solution, when the anode is switched to the inert electrode, the injected tellurium is consumed at the cathode forming CdTe. This is necessary to control the $HTeO_2^+$ concentration, $[HTeO_2^+]$, in the electrolyte. The Cd^{2+} concentration can be controlled by using a cadmium anode or by replenishing the electrolyte whenever needed. The 0.5 M $CdSO_4$ solution is purified for at least 2 h using a platinum cathode before the introduction of the tellurium The solution temperature is kept around 85 - 90 °C during this pre-electrolysis period. After adjusting the pH to around 1.6, 30 - 40 ppm of $HTeO_2^+$ is introduced into the electrolyte by applying a potential of about 500 mV to the tellurium anode with respect to an Ag/AgCl reference electrode The cathode for the CdTe plating process consists of a metallized or a TCO-coated glass substrate or a glass/TCO/CdS substrate depending upon the desired device structure. The quasi-rest potential [11, 12] of the deposit is kept at a value right below where pure cadmium deposition takes place.

The deposition of CdTe on the cathode can be accomplished by the following reactions:

$$HTeO_2^+ + 3H^+ + 4e^- \longrightarrow Te + 2H_2O$$

$$Cd^{2+} + Te + 2e^- \longrightarrow CdTe$$

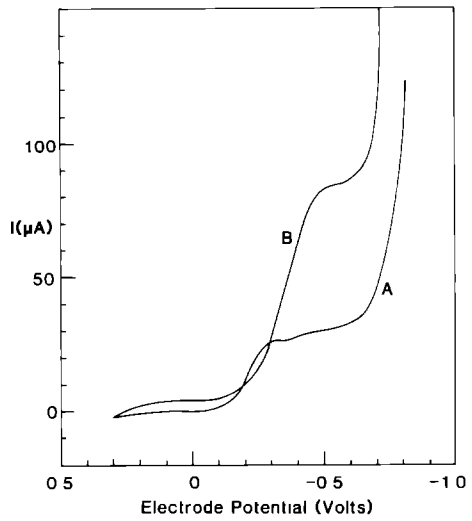

Fig. 2 Voltammograms for tellurium (curve A) and CdTe (curve B) electrodeposition.

Figure 2 shows the voltammograms taken from two experimental electrolytes. The voltage scale in this figure indicates the cathode potential measured with respect to an Ag/AgCl reference electrode. Curve A in Fig. 2 was obtained using a solution containing 32 ppm of $HTeO_2^+$ in 0.5 M Na_2SO_4 as the supporting electrolyte. The first rise in the current at around −0.2 V illustrates the formation of tellurium on the cathode. The rise in the current for voltages above −0.7 V can be due either to the reduction of the deposited tellurium to H_2Te or to the hydrogen evolution. Curve B is a voltammogram taken from an electrolyte containing 23 ppm of $HTeO_2^+$ and 0.5 M $CdSO_4$. The observed current at the tellurium deposition potentials is higher compared with that shown on curve A despite the fact that the $[HTeO_2^+]$ is lower for the electrolyte of curve B. This indicates that CdTe deposition takes place for cathode potentials between −0.2 and −0.65 V.

After the publication of the original paper by Panicker *et al.* [10] several groups have studied the cathodic deposition process for CdTe. A good review of this work and a kinetic model for the electrodeposition of CdTe are given by Engelken and Van Doren [36].

The deposition current density for CdTe plating depends on the tellurium concentration in the electrolyte, the rate of stirring and the deposition temperature. Typical current density values for the present work were 0.3 - 0.5 mA cm^{-2}. The deposition rate was in the range 120 - 180 Å min^{-1}.

3 3. HgCdTe deposition

The procedure for HgCdTe electrodeposition is similar to that for CdTe deposition. The only difference is the addition of Hg^{2+} ions (using $HgCl_2$) to the electrolyte after the introduction of $HTeO_2^+$ as described above. Curve F in Fig. 3 is a voltammogram taken from a solution containing 10 ppm of Hg^{2+}, 32 ppm of $HTeO_2^+$ and 0.5 M Na_2SO_4. Curve E, which represents the

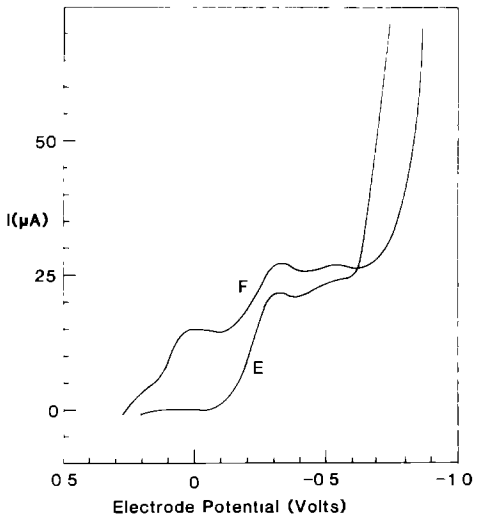

Fig. 3. Voltammograms for tellurium (curve E) and HgTe (curve F) electrodeposition

tellurium deposition, is repeated here for comparison. The mercury deposition wave in curve F appears at voltages more positive than that of the tellurium deposition. It is clear from this figure that CdTe and mercury can be codeposited on the cathode at voltages between −0.4 and −0.65 V.

Figure 4 shows the mercury-to-tellurium atomic ratios, $(1-x)$, of 16 different electrodeposited $Hg_{(1-x)}Cd_xTe$ films as a function of the electrolyte composition. These measurements were made using an atomic absorption spectrophotometer (AAS). The points in Fig. 4 represent the Hg^{2+}:$HTeO_2^+$ ratios measured for the electrolytes before the plating of the films. Arrows indicate the change in these ratios during plating. This change is due to the depletion of Hg^{2+} in the electrolyte. The vertical bars show the variation in the mercury-to-tellurium ratio on different parts of a given

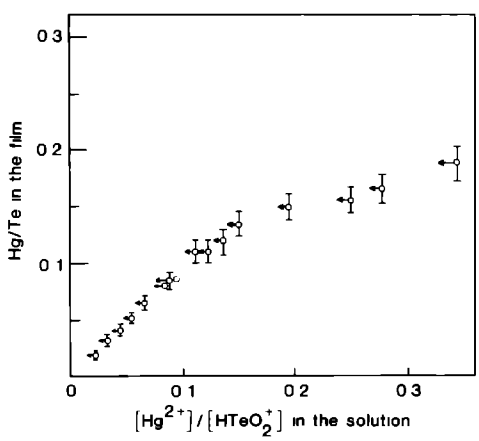

Fig 4. Stoichiometry of the electrodeposited HgCdTe films as a function of the electrolyte composition

sample and the error involved in the AAS measurements. It should be noted that the depletion of Hg^{2+} ions from the electrolyte and the resulting stoichiometric changes through the thickness of the plated films can be avoided if Hg^{2+} is continuously fed into the electrolyte in the same way as $HTeO_2^+$. It should also be noted that the accuracy of the data in Fig. 4 is reduced in the high mercury concentration region. This is partly due to the expected loss of some Hg^{2+} to an exchange reaction taking place with the tellurium anode and partly due to the appearance of a mercury-rich powdery deposit on the surface of the films with high $(1-x)$ values. The data in Fig. 4 were taken after wiping such powdery deposits off the surface of the films.

3.4. The TCJF process

The as-deposited films described in Sections 3.2 and 3.3 are high resistivity (typically $10^4 - 10^6\ \Omega$ cm) n-type materials. The high efficiency heterojunction structures, however, require the use of p-type layers.

Although the electrical type of the plated CdTe films can be changed by controlling the deposition potential [10, 11], our experience so far has indicated that the p-CdTe films prepared this way contain free tellurium as a second phase. Takahashi *et al.* [37], for example, claim a sheet resistance of 1 - 8 Ω for their electroplated p-CdTe layers. Although the film thickness was not indicated in this reference, the given sheet resistance value translates into a CdTe resistivity in the range of $10^{-4}\ \Omega$ cm for a typical 1 μm thick film. In a more recent paper the same researchers report on as-deposited p-CdTe films with a resistivity of 1 - 3 Ω cm [38]. The conductivity of such CdTe tellurium films decreases sharply upon heat treatment at temperatures above 200 °C. This is due to the loss of elemental tellurium. As for the extrinsic doping, copper was found to be the most effective p-type dopant for our films. However, no efficient device has been demonstrated so far on as-deposited copper-doped films. On the basis of the information presented above, we conclude that it would be extremely difficult to electroplate a solar cell grade p-CdTe layer which would yield high efficiency devices in its as-deposited form.

To overcome the problems associated with obtaining solar cell grade as-deposited p-CdTe layers, the Monosolar team has developed a TCJF process [31, 35, 39]. In this technique a high resistivity n-CdTe film is electrodeposited on the glass/TCO/CdS substrate to a thickness of 1.0 - 1.5 μm. The glass/TCO/CdS/CdTe structure is then heat treated in air at around 400 °C for 8 - 12 min. During the TCJF process the n-CdTe layer is converted into solar cell grade p-CdTe and the rectifying junction is formed *in situ*, between the CdS film and the converted CdTe layer. The process is the same for the electrodeposited HgCdTe films.

Figure 5(a) shows the spectral response data taken from the glass/ITO/CdS/Au devices (measurements made through the glass substrate) as a function of the TCJF annealing time. The annealing temperature (350 °C) in this experiment was selected below the optimum value of 400 °C in order

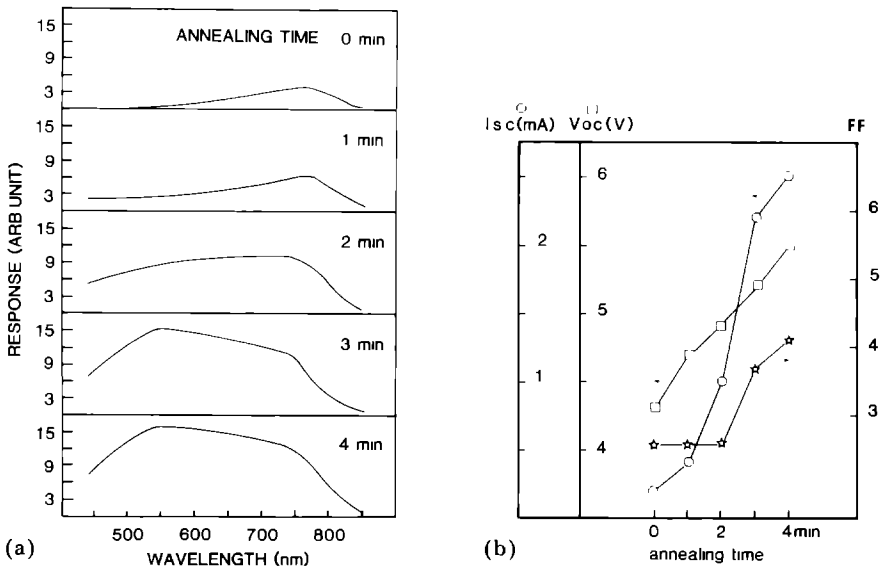

Fig. 5 (a) Spectral response of a glass/ITO/CdS/CdTe/Au device as a function of the annealing time (annealing temperature, 350 °C, device area, 0.02 cm^2). (b) Solar cell parameters for the devices in (a): ○, short-circuit current; □, open-circuit voltage, ☆, fill factor

to slow down the conversion process. Figure 5(b) shows the solar cell parameters for the same devices. An appreciable rise in the short-wavelength response in the early stages of the heat treatment, a flattening of the response for times of around 2 min and the eventual shift of the response peak to the short-wavelength region is clearly observed in the spectral response data. This is indicative of the junction moving from its initial position at the Au/CdTe interface to the CdS/CdTe interface. The final location of the junction is determined by the heat treatment time and temperature, residual impurities in the CdTe film and any impurities which may be diffusing into the CdTe from the glass/ITO/CdS substrate. In other words, if the residual donor density in the CdTe film was high and/or donor impurities (such as indium) had diffused to the interface from the ITO layer, a buried homojunction could be formed. For the films used in this experiment, the sharp improvements in both the fill factor and the short-circuit current values of the cells coincide with the shift of the response peak after 3 min of heat treatment. The possible mechanisms for the observed type conversion in CdTe, such as the acceptor impurity diffusion from the annealing atmosphere, the substrate or the grain boundaries, were evaluated in ref. 39. We believe that the intrinsic defects play the major role in the TCJF process. Possible intrinsic defects in CdTe are cadmium vacancies, cadmium interstitials, tellurium vacancies and tellurium interstitials. Cadmium vacancies and tellurium interstitials are expected to act as acceptors and others as donors. The as-deposited n-CdTe is a highly compensated material. Its electrical properties are dominated by residual impurities, cadmium interstitials and/or tellurium vacancies. When this material is heated under a low

cadmium overpressure, depletion of cadmium interstitials (donors) and creation of cadmium vacancies (acceptors) occur. Since isolated native defects have a very high mobility in CdTe [40], the cadmium vacancies are most probably associated with impurities forming compensating acceptor complexes. It should be noted that the residual donor impurities in the plating electrolyte have a strong influence over the TCJF process. In one experiment, n-CdTe films obtained from an electrolyte containing over 500 ppm of Br^-, a known donor in CdTe, could not be converted into p type even after heat treatment for 10 min at 400 °C. It is for this reason that the time for the onset of the type conversion indicated in Figs. 5(a) and 5(b) is a sensitive function of the residual impurities in the film. However, for films obtained from properly purified electrolytes the type conversion always occurs. Effects of the residual impurities become more important for high efficiency cells where the resistivity of the type-converted film plays an important role in the device performance.

Oxygen is known to be a necessary ingredient in the p-type CdTe layers prepared by the close-spaced sublimation (CSS) method [41]. Although it is known that oxygen introduces acceptor states in these films, the form of these acceptors is not clear. Does oxygen act as a simple acceptor, or does it form acceptor complexes with native defects? Does it help the creation of cadmium vacancy acceptors by acting as a sink for cadmium? Does it fill in the tellurium vacancies? These are issues that are being addressed, especially by groups working with the CSS technique because CSS is a method that allows the introduction of controlled amounts of oxygen into the CdTe film during growth [41, 42]. Another important question which needs to be addressed is whether the oxygen effect is a bulk or a surface phenomenon.

Our electrodeposited CdTe films were prepared in aqueous solutions and they already contained oxygen before they were subjected to the TCJF process. Therefore it is rather hard to isolate the effect of the oxygen already existing in the film from the effect of the oxygen in the annealing environment. We can state, however, that although the type conversion for our films could be achieved by heat treating the films in various atmospheres including hydrogen, the cells made on air-annealed CdTe films had, on the average, better fill factors and better efficiencies. In the following paragraphs we will present data pertaining to the effect of oxygen on the ohmic contacts made to the electroplated CdTe films.

Figure 6 shows the illuminated $I-V$ characteristics of three experimental devices prepared for the study of the effect of oxygen on the commonly used gold contacts. The devices were prepared as follows [39]:

(a) Electrodeposited CdS/CdTe heterojunctions were obtained using the TCJF process.

(b) After etching in 0.1 vol.% bromine in methanol, the glass/ITO/CdS/CdTe structure was put in a vacuum system, heated up to 300 °C in 2 min and then cooled down to room temperature. The pressure was in the 10^{-6} Torr range. Gold contacts of thickness 200 Å were evaporated onto the CdTe surface (curve A in Fig. 6).

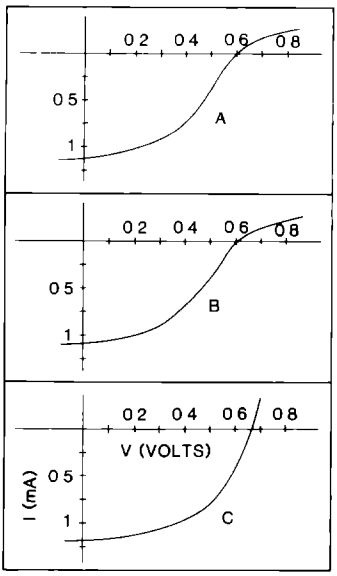

Fig. 6. Illuminated $I-V$ characteristics of a glass/ITO/CdS/CdTe/Au device (device area, 0.07 cm^2): curve A, after annealing in vacuum and depositing the gold contact; curve B, after 72 h of storage in nitrogen, curve C, after 72 h of storage in air

(c) Devices were stored in either nitrogen or air and their illuminated characteristics were measured (curves B and C).

The details of this experiment are given in ref. 39. It is clear from Fig. 6 that the presence of oxygen in the device environment is necessary to eliminate a barrier which occurs at the Au/CdTe interface as a result of the vacuum annealing step. It should be noted that similar heat treatments carried out in air before the gold contact evaporation did not give rise to such high contact barriers in these devices. The results of this study can be explained by the acceptor properties of oxygen. Oxygen may be chemisorbed at the surface of the CdTe giving rise to acceptor states which would bend the bands up to reduce the surface barrier at the Au/CdTe interface. Using the same argument for the grain boundaries of our polycrystalline CdTe films, we can see that the bulk electrical characteristics of small grains can be strongly influenced by the height of the barriers at their boundaries, *i.e* a decrease in the band bending at the grain boundaries can push the Fermi level in the grain closer to the valence band. Therefore, a possible model for the TCJF process can be the out-diffusion of cadmium from the bulk of the grains to the grain boundaries and the chemisorption of oxygen at these surfaces. In this way, cadmium vacancy acceptors are created in the bulk of the grains and the band bending is partially controlled by the oxygen at the grain boundaries.

3.5. Ohmic contacts

After the type conversion and junction formation, the last step in the device processing is the back-contact deposition. The quality of ohmic

contacts to p-CdTe is very much dependent on the surface stoichiometry of CdTe and a tellurium-rich surface is generally required for low contact resistivity [40]. The contact metals we have commonly used for our devices were gold and nickel. Nickel contacts were found to be more stable than the gold contacts. One important reason for the observed thermal instability of the gold contact is the interaction between the CdTe surface and the gold which gives rise to stoichiometric changes on the CdTe surface. We have used Auger analysis to study the Au–CdTe interaction in our devices. Table 1 gives the relative Auger intensity data for the elements detected on the surface of gold contacts which were vacuum evaporated onto the electrodeposited CdTe surfaces. The CdTe surface for sample B was freshly etched in a bromine–methanol solution before the gold evaporation. Samples C, D and E were stored in air for 24 h, heat treated in nitrogen for 24 h and heat treated in air for 24 h respectively. The most important observation from Table 1 is the existence of tellurium on the surface of the evaporated gold contacts even before any post-deposition heat treatment. Apparently, the tellurium concentration builds up at the surface of the gold as the latter is evaporated onto the CdTe surface. The existence of cadmium on the heat-treated contact surfaces further suggests that both tellurium and cadmium diffuse through the gold contact and eventually form a Cd_xTe_y alloy at the top surface of the gold (see data for sample E). The Auger depth profile through the gold contact of sample B also shows that the Au–Te interaction removes the excess tellurium from the etched CdTe surface (Fig. 7). This change in the surface stoichiometry explains why bromine–methanol etching coupled with gold contacts has given poor fill factors in our devices.

The procedure which gave the best contact resistivity in our electrodeposited solar cells was [43]: (i) etching the CdTe surface with an oxidizing etch such as chromic acid which gives a tellurium-rich surface layer 300 - 500 Å thick, (ii) immersing the etched surface in hydrazine which removes a high resistivity tellurium oxide film from the top of the surface layer.

TABLE 1

Relative Auger intensity of elements detected on the evaporated gold contact for various samples

Sample	*Relative intensity* (%)						
	Au	*Cd*	*Te*	*O*	*C*	*Cl*	*S*
B[a]	48.6	0	34 1	4	13.3	0	0
C[b]	45	0	33.6	3.9	10.2	0	7.2
D[c]	6.2	29.2	33.6	17 1	9	3.6	1.3
E[d]	0	34 9	32.7	18.8	8 9	4.1	0.5

[a]Sample etched in bromine–methanol and gold evaporated.
[b]Sample stored at room temperature for 24 h.
[c]Sample heat treated in nitrogen for 24 h.
[d]Sample heat treated in air for 24 h.

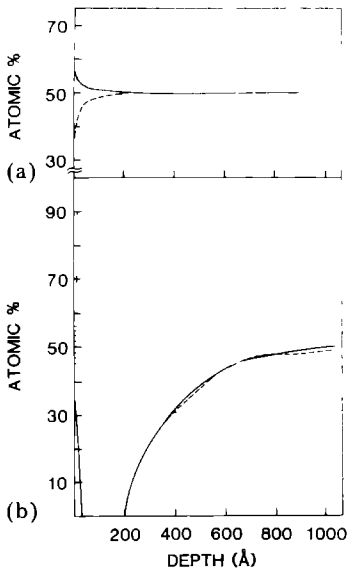

Fig. 7 (a) Auger depth profile for a p-CdTe film etched in bromine–methanol (sample B) ——, tellurium, — — —, cadmium. (b) Auger depth profile taken through the gold contact on sample B ·· ·, gold; ——, tellurium; — — —, cadmium

It should be noted that the hydrazine step does not remove all the tellurium oxide from the surface region which is 300 - 500 Å thick. The Auger profile shows the existence of TeO_x + tellurium in this region.

4. Film characterization

4.1. Structural properties

The electrodeposited CdS films are 500 - 1000 Å thick and they have a hexagonal structure. The grain size in these films is about equal to the thickness of the film. The resistivity of the CdS layers is typically 50 - 500 Ω cm.

As-deposited CdTe films are polycrystalline with grain sizes of the order of 0.5 - 1 μm for films 1 - 1.5 μm thick. They have the cubic structure with a (111) preferred orientation [10]. The surface has a nodular texture typical of solution-grown films [10]. Electrodeposited $Hg_{1-x}Cd_xTe$ films show different structural characteristics [17]. The surface under scanning electron microscopy looks more granular and the grains are larger than those in the CdTe films. Figure 8 shows the X-ray diffraction data taken from two electrodeposited $Hg_{1-x}Cd_xTe$ films with $(1-x) = 0.08$ and $(1-x) = 0.16$. One interesting observation from these X-ray patterns is the apparent loss of the (111) preferred orientation in the films as $(1-x)$ increases. This is a reflection of the change in the nucleation and the growth processes for the HgCdTe films as compared with those for the CdTe films. Since mercury is the first depositing species in the HgCdTe plating bath, it is expected that

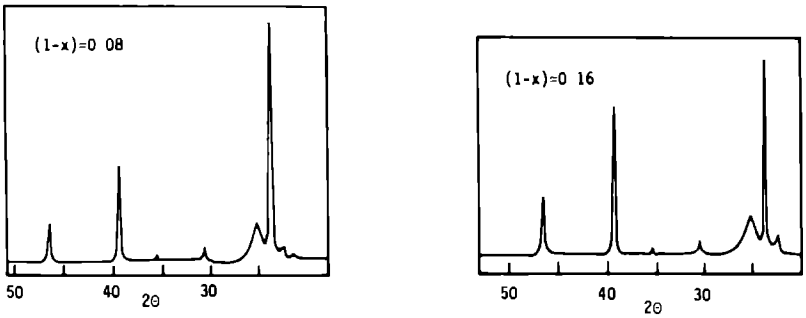

Fig. 8. X-ray diffraction data for $Hg_{(1-x)}Cd_xTe$ films.

the region of the film near the CdS surface is higher in mercury content and it is also expected that the density of the mercury-rich nucleation sites on the CdS surface is a strong function of the Hg^{2+} concentration in the electrolyte. Five peaks in the back-reflection area of the X-ray diffraction data were measured for the samples of Fig. 8 and the average cubic cell edge, a_1, was calculated. The a_1 values for the samples with low and high mercury content were 6.483 Å and 6.479 Å respectively. This is an expected trend going from CdTe to HgCdTe. The sample with a high mercury content also showed sharper peaks in the back-reflection area indicating a larger grain size for this sample.

4.2. Optical and electrical characteristics

Optical properties of as-deposited n-type and type-converted p-type CdTe films have been studied [27, 44]. The optical absorption coefficients and the index of refraction for these CdTe films are given in Figs. 9(a) and 9(b). It should be noted that the measured optical absorption near the band edge is higher for the type-converted films than for the as-deposited layers. This may be a result of defect absorption [44].

The dependence of the optical band gap of the electrodeposited $Hg_{(1-x)}Cd_xTe$ films on their stoichiometry is shown in Fig. 10. The data were obtained from the transmission and reflection measurements made on thin films [16]. It is observed that the band gap values follow the expected linear dependence on $(1-x)$ within the limits of experimental error.

The resistivity of as-deposited n-CdTe films is in the range 10^4 - 10^6 Ω cm. Type-converted p-CdTe layers used in our work had resistivities in the range (5×10^4) - (5×10^5) Ω cm. The HgCdTe resistivity is a strong function of its stoichiometry. For $(1-x)$ higher than 0.15 we can get resistivities in the range of 10^3 Ω cm. The conductivity of electrodeposited HgCdTe is dominated by the mercury vacancy defects which are generated during the TCJF process. Since the Hg—Te bond is weaker than the Cd—Te bond, mercury vacancies are easier to form than the cadmium vacancies and they introduce shallow acceptor levels near the valence band.

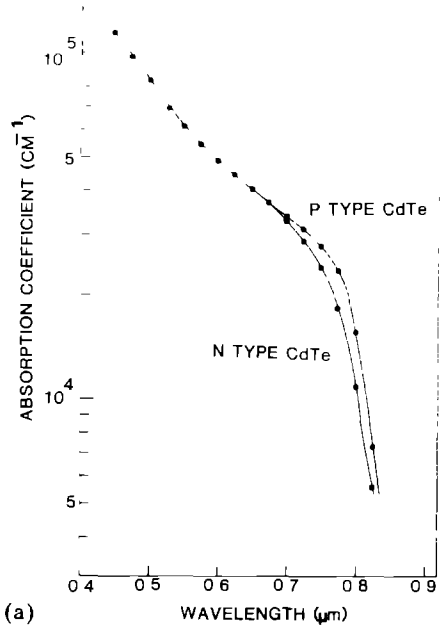

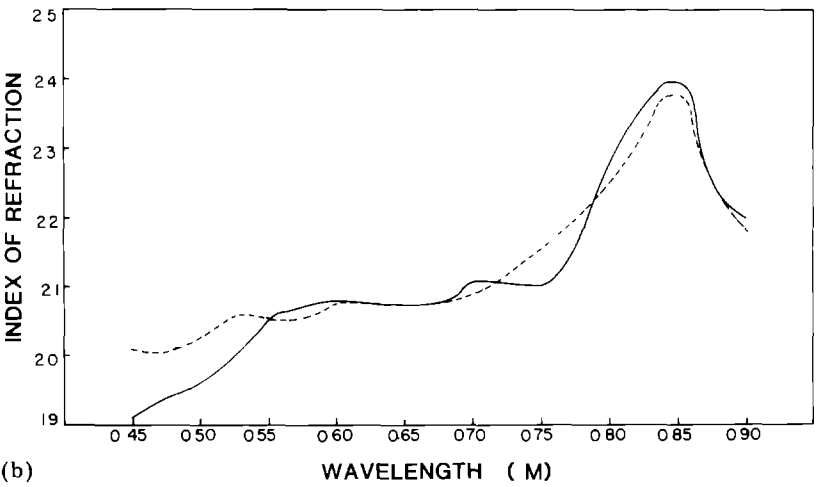

Fig. 9. (a) Optical absorption coefficients for electrodeposited n-type and p-type films. (b) Index of refraction for electrodeposited CdTe films. — — —, p type, ——, n type.

Electrical properties of CdTe and HgCdTe thin films are dominated by intrinsic defects. These materials are highly compensated where the native defects, residual impurities and the interaction between the two play an important role in determining the overall properties. The defect structures of electrodeposited CdTe and HgCdTe films are not yet completely understood. Table 2 gives the results of some defect studies carried out by our group on the as-deposited and type-converted CdTe films. The measurement

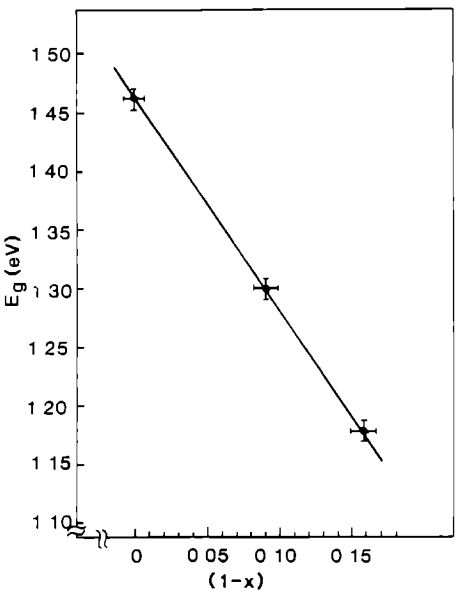

Fig. 10 Optical band gap of electrodeposited $Hg_{(1-x)}Cd_xTe$ films.

techniques and the references [25, 26, 45, 46] are also given. The deep levels at around $E_c = -0.55$ eV in the as-deposited n-CdTe films have been associated with the cadmium interstitials which are expected to exist in films grown under cadmium-rich conditons. The $(E_v + 0.54)$-eV level in the type-converted high resistivity p-type CdTe film was found to be a hole trap with a capture cross-section of 1.1×10^{-13} cm^2 and it may be associated with the doubly ionized cadmium vacancies which are expected to form as a result of the TCJF process. The $(E_v + 0.2)$-eV level, however, corresponds to a cadmium vacancy–impurity complex. The $(E_v + 0.35)$-eV level is attributed to residual acceptor impurities.

TABLE 2

Observed defect levels in electrodeposited CdTe films

Film type	*Energy level*	*Measurement method*	*Reference*
n-CdTe	$E_c - 0.55$	SCLC[a]	25
	$E_c - 0.56$	Cap[b]	26
p-CdTe	$E_v + 0.54$	DLTS[c]	45
	$E_v + 0.35$	DLTS[c]	45
	$E_v + 0.2$	PL[d]	45
	$E_v + 0.54$	SCLC[a]	46

[a]Space-charge-limited currents.
[b]Capacitance measurements.
[c]Deep-level transient spectroscopy.
[d]Photoluminescence.

5. Heterojunction devices

5.1. Characterization

The study of current transport mechanisms in electrodeposited CdS/CdTe devices is described in ref. 47. Multistep tunneling was found to be the dominating mechanism for temperatures between 200 and 350 K. The capacitance measurements on CdS/CdTe devices showed an appreciable frequency and illumination dependence [48] indicating the dominance of deep levels and surface states in these cells. Figure 11 shows typical $1/C^2$ data for CdS/HgCdTe devices with different stoichiometries. The observed non-linearity in the CdTe cell capacitance data is typical and it is due to the fact that the resistivity of this material is determined by deep levels which cannot respond to the signal frequency. It should be noted that the $1/C^2$ curves for the CdTe devices approach linearity and they show stronger bias dependence when the measurement frequency is reduced below 10 Hz or the measurement is done under light bias [48]. The HgCdTe devices, however, show normal linear $1/C^2$ behaviour as their stoichiometry becomes more and more mercury-rich. This is indicative of the shallow mercury-vacancy-related acceptor levels in these materials. The ionized charge density values calculated from the capacitance curves of Fig. 11 change from 6×10^{15} in curve A to 3×10^{16} in curve C. The dark and illuminated capacitance values measured for our devices indicate that the depletion region does not extend all the way through the CdTe and HgCdTe films especially when these devices are under illumination. This is contrary to a recent report on a CdS/CdTe cell where a completely depleted CdTe layer is suggested [49].

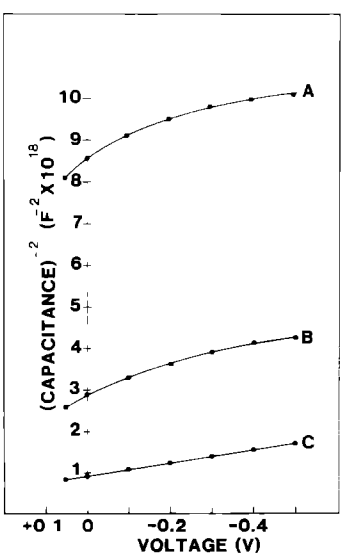

Fig. 11 $1/C^2$ *vs.* V characteristics for $Hg_{(1-x)}Cd_xTe$ devices. $(1-x)$ is 0, 0 09 and 0.16 for devices A, B and C respectively (device area, 0 02 cm^2).

The device in ref. 49 used the TCJF process described in this paper and utilized a ZnTe layer contact with the type-converted CdTe film. Capacitance, photocapacitance and spectral response measurements are needed to determine the type of the device in ref. 49.

Figures 12 and 13 show the $I-V$ characteristics of two high efficiency electroplated CdTe and HgCdTe solar cells under air mass (AM) 1.5 illumination. Both of these cells had nickel back contacts. The solar cell parameters for the CdTe device are J_{sc} = 21.23 mA cm^{-2}, V_{oc} = 0.725 V, FF = 0.67 and efficiency, 10.31% (area, 0.16 cm^2). The $Hg_{0.1}Cd_{0.9}Te$ cell shown in Fig. 13 has J_{sc} = 27.03 mA cm^{-2}, V_{oc} = 0.620 V, FF = 0.633 and efficiency, 10.6% (area, 1.48 cm^2). It should be noted that the best solar cell parameters observed in our electroplated CdTe devices were 0.82 V for V_{oc}, 23 mA cm^{-2} for J_{sc} and 0.68 for FF. The J_{sc} and V_{oc} values for the HgCdTe devices are strongly dependent on the stoichiometry of the material, but the highest FF observed for these cells was 0.70. HgCdTe has the advantage of having a lower resistivity than CdTe. It is our experience that good fill factors in large-area HgCdTe cells are more reproducible than in CdTe devices [20].

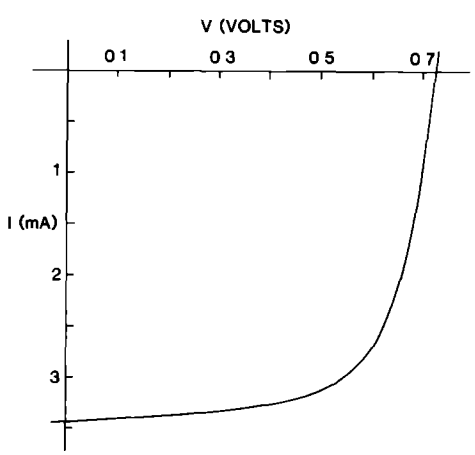

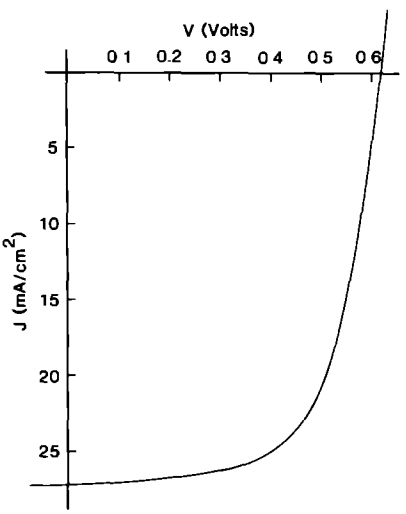

Fig. 12. Illuminated $I-V$ characteristics of an electrodeposited CdS/CdTe device (area, 0.16 cm^2): J_{sc} = 21.23 mA cm^{-2}; V_{oc} = 0.725 V; FF = 0.67; AM 1 5, illumination, 100 mW cm^{-2}. The efficiency is 10.31%.

Fig. 13. Illuminated $I-V$ characteristics of an electrodeposited $Hg_{0.1}Cd_{0.9}Te$ device (area, 1.48 cm^2): J_{sc} = 27.03 mA cm^{-2}; V_{oc} = 0.62; FF = 0.633; AM 1.5, illumination, 100 mW cm^{-2}. The efficiency is 10.6%.

6. Conclusions

As-deposited p-CdTe films do not yield high efficiency photovoltaic devices. The key step in obtaining high efficiency electrodeposited CdTe and HgCdTe thin film solar cells is the TCJF process described in this paper.

The results presented in Section 5 establish the electrodeposited CdTe and HgCdTe solar cell technology as one of the most important thin film photovoltaic technologies of today. The solar cell parameters given above indicate that the current collection in these devices is quite good Further improvements in the fill factor and open-circuit voltage values are expected. The improvement in the fill factor mainly depends on the improvement in the contact resistivity. This can be achieved by extrinsic doping of the films in addition to the defect doping achieved by the TCJF process. Another approach for improving the contact resistivity is the use of metal–telluride buffer layers between the contact metal and the CdTe film [20, 49]. In this case, partial doping of the CdTe layer can be achieved by diffusing the dopants from the buffer layer into the CdTe. High contact resistivity is less of a problem for the lower resistivity HgCdTe films but the fill factors can still be improved by doping. It is expected that marginal improvements in the fill factor values will allow, in the near future, the production of over 12% efficient electrodeposited CdTe and HgCdTe thin film solar cells.

Acknowledgments

The work reported in this paper is the result of efforts by many people. The author wishes to acknowledge the contributions to this work by his colleagues at Monosolar, Dr. Robert L. Rod, Eric S. Tseng, Dennis S. Lo, Ricardo Campos and Walter Penick and at UCLA, Professor Oscar M. Stafsudd and Dr. Simon S. Ou. Valuable comments by Dr. Vijay K. Kapur of ISET are greatly appreciated.

Monosolar's electrodeposited CdTe and HgCdTe solar cell technology was transferred to British Petroleum/The Standard Oil of Ohio in mid-1984 where it is under further development. This author and his colleagues at ISET are presently persuing other approaches involving electrodeposition for the preparation of II–VI and I–III–VI_2 compounds for solar cell applications. ISET's present research efforts are directed towards the development of high efficiency copper indium diselenide ($CuInSe_2$) and higher band gap (CdZn)Te devices for single-junction and tandem-junction solar cells.

References

1 J. J Loferski, *J. Appl. Phys.*, *27* (1956) 777.
2 R W Birkmire, L C. DiNetta, S C. Jackson, P. G. Lasswell, B. E. McCandless, J. D. Meakin and J. E. Phillips, *Proc 18th IEEE Photovoltaic Specialists' Conf., Las Vegas, NV, 1985*, IEEE, New York. 1985, p. 1413.
3. H. Uda, H. Taniguchi, M. Yoshida and T. Yamashita, *Jpn. J. Appl Phys*, *17* (1978) 585
4 M. B. Das, S. V. Krishnaswamy, R. Petkie, P Swab and K. Vedam, *Solid-State Electron.*, *27* (1984) 329
5 Y S. Tyan and E. A. Perez-Albuerne, *Proc. 16th IEEE Photovoltaic Specialists' Conf., San Diego, CA, 1982*, IEEE, New York, 1982, p. 794.

6 K. W. Mitchell, C. Eberspacher, F. Cohen, J. Avery, G. Duran and W. Bottenberg, *Proc. 18th IEEE Photovoltaic Specialists' Conf., Las Vegas, NV, 1985*, IEEE, New York, 1985, p. 1359.

7 H. Uda, H. Matsumoto, Y. Komatsu, A. Nakano and S. Ikegami, *Proc. 16th IEEE Photovoltaic Specialists' Conf., San Diego, CA, 1982*, IEEE, New York, 1982, p. 801.

8 H. B. Serreze, S. Lis, M. R. Squillante, R. Turcotte, M. Talbot and G. Entine, *Proc. 15th IEEE Photovoltaic Specialists' Conf., Orlando, FL, 1981*, IEEE, New York, 1981, p. 1068

9 T. L. Chu, S S. Chu, F. Firszt, H. A. Naseem, R. Stawski and G Xu, *Proc. 18th IEEE Photovoltaic Specialists' Conf., Las Vegas, NV, 1985*, IEEE New York, 1985, p. 1643

10 M. P. R. Panicker, M Knaster and F A. Kroger, *J. Electrochem Soc., 125* (1978) 556

11 F A Kroger, R L. Rod and M. P. R Panicker, Photovoltaic power generating means and methods, *U S Patent 440 02 44, August 1983*,
F A Kroger and R. L. Rod, *U.K. Patent 153 26 16*, February 1979.

12 K. Zweibel, R Mitchell and A Hermann, *Proc 18th IEEE Photovoltaic Specialists' Conf., Las Vegas, NV, 1985*, IEEE, New York, 1985, p. 1393.

13 R H. Bube, in J A. Amick, V. K. Kapur and J. Dietl (eds.), *Materials and New Processing Technologies For Photovoltaics*, Vol. PV 83-11, Electrochemical Society, Pennington, NJ, 1983, p. 359.

14 C. Cohen-Solal, M. Barbe, H Afifi and G. Neu, *J Cryst. Growth, 72* (1985) 512.

15 P W Kruse, in R K. Willardson and A C. Beer (eds), *Semiconductors and Semimetals*, Vol. 18, Academic Press, New York, 1981, p 1

16 B. M. Basol, O. M. Stafsudd and A. Bindal, *Sol. Cells, 15* (1985) 279

17 B. M Basol, E. S. Tseng and O. M. Stafsudd, *Proc. 18th IEEE Photovoltaic Specialists' Conf, Las Vegas, NV, 1985*, IEEE, New York, 1985, p. 1745

18 B. M. Basol, E S Tseng and D. S. Lo, Electrodeposition of thin film heterojunction photovoltaic devices that utilize Cd-rich $Hg_{(1-x)}Cd_xTe$, *U S Patent 454 86 81*, October 1985

19 B. M. Basol, E S Tseng and D. S. Lo, Thin film heterojunction photovoltaic devices, *U S. Patent 462 98 20*, December 1986

20 B M Basol and E. S. Tseng, *Appl Phys Lett., 48* (1986) 946.

21 R. L. Rod and F A Kroger, *Proc ERDA Semiannual Solar Photovoltaic Program Review Meeting, Orono, Maine, August 3 - 6, 1976*, National Technical Information Service, Springfield, VA, 1976, p. 401.

22 R. L. Rod, M. Knaster, F A. Kroger and K Lehovec, *Proc SERI/DOE Photovoltaics Advanced Materials Review Meeting, Denver, CO, October 24 - 26, 1978*, National Technical Information Service, Springfield, VA, 1979, p. 485.

23 K Mitchell, *Proc. SERI/DOE Photovoltaics Advanced R&D Annual Review Meeting, September 17 - 19, 1979*, National Technical Information Service, Springfield, VA, 1979, p. 387

24 B. M Basol, *Ph.D. Dissertation*, University of California, Los Angeles, 1980.

25 B. M. Basol and O. M Stafsudd, *Solid-State Electron., 24* (1981) 121.

26 B. M Basol and O. M. Stafsudd, *Thin Solid Films, 78* (1981) 217.

27 B. M. Basol and O. M. Stafsudd, *Appl Phys. Lett., 38* (1981) 918.

28 Z. Shkedi and R. L. Rod, *Proc. 14th IEEE Photovoltaic Specialists' Conf., San Diego, CA, 1980*, IEEE, New York, 1980, p. 472

29 B M Basol, O. M. Stafsudd, R L. Rod and E. S Tseng, *Proc. 3rd Commission of the European Communities Conf on Photovoltaic Solar Energy*, Reidel, London, 1980, p. 878.

30 G. Fulop, M. Doty, P. Meyers, J. Betz and C H. Liu, *Appl. Phys Lett., 40* (1982) 327

31 B. M Basol, E S. Tseng and R. L. Rod, Thin film heterojunction photovoltaic cells and methods of making the same, *U.S. Patent 438 84 83*, June 1983

32 B M. Basol, R L Rod and E. S. Tseng, *Proc 4th Commission of the European Communities Conf. on Photovoltaic Solar Energy*, Reidel, London, 1982, p 719
33 B M Basol, E. S Tseng, R L. Rod, S S. Ou and O. M. Stafsudd, *Proc 16th IEEE Photovoltaic Specialists' Conf., San Diego, CA, 1982*, IEEE, New York, 1982, p. 805.
34 B M Basol and E S Tseng, in J A. Amick, V. K. Kapur and J. Dietl (eds), *Materials and New Processing Technologies for Photovoltaics*, Electrochemical Society, Pennington, NJ, 1983, p. 463
35 B. M. Basol, *J. Appl Phys., 55* (1984) 601.
36 R D Engelken and T P. Van Doren, *J. Electrochem. Soc., 132* (1985) 2910.
37 M. Takahashi, K. Uosaki and H. Kita, *J. Appl. Phys., 55* (1984) 3879
38 M. Takahashi, K. Uosaki and H. Kita, *J Appl Phys , 60* (1986) 2046.
39 B. M. Basol, S. S. Ou and O. M Stafsudd, *J. Appl Phys , 58* (1985) 3809.
40 K. Zanio, in R. K Willardson and A. C. Beer (eds), *Semiconductors and Semimetals*, Vol. 13, Academic Press, New York, 1978, p 115.
41 Y S Tyan, F Vazan and T S. Barge, *Proc 17th IEEE Photovoltaic Specialists' Conf , Kissimmee, FL, 1984*, IEEE, New York, 1984, p 840.
42 T M Hsu, R J Jih, P. C Lin, H Y Ueng, Y J Hsu and H L Hwang, *J Appl. Phys , 59* (1986) 3607
43 B. M. Basol, Method of forming ohmic contacts, *U S. Patent 445 66 30*, 1984.
44 S. S. Ou, O M Stafsudd and B. M Basol, *J Appl. Phys , 55* (1984) 3769
45 S S. Ou, A Bindal, O M. Stafsudd, K. L Wang and B M Basol, *J Appl. Phys., 55* (1984) 1020.
46 S S. Ou, O. M Stafsudd and B. M. Basol, *Thin Solid Films, 112* (1984) 301.
47 S S. Ou, O M Stafsudd and B M. Basol, *Solid-State Electron., 27* (1984) 21.
48 L. J. Cheng, T. T. Nguyen, C. M Shyu, B. M. Basol and H. I Yoo, *Proc 17th IEEE Photovoltaic Specialists' Conf., Kissimmee, FL, 1984*, IEEE, New York, 1984, p 851
49 P. V. Meyers, *Proc 7th Commission of the European Communities Conf. on Photovoltaic Solar Energy*, Reidel, London, 1986, p 1211.